University of Twente

Experimental demonstration of reduced bend losses in low-contrast polymer hybrid waveguides

W.E. van de Meent

January 2015

Experimental demonstration of reduced bend losses in low-contrast polymer hybrid waveguides

W.E. van de Meent

Bachelor of Science thesis
January 2015

University of Twente
Faculty of Science and Technology
Optical Sciences

Graduation committee:
Prof. Dr. J.L. Herek
Dr. E.S. Kooij
M.A. Sefunc, M.Sc.

Abstract

In the pursuit of smaller and smaller optical devices, efficient waveguides are desired for signal transmission and sensing applications. New waveguide designs should meet economic criteria as well as technical requirements: they have to be energy-efficient and processable on micrometer scale.

Polymer waveguides have been proposed as a good candidate for integrated optical circuitry, because they are easy to fabricate at low cost. Also polymer materials span a wide range of refractive index values, and they exhibit a large transparency window. But unfortunately such waveguides show relatively high radiation losses in sharp bends, which until now has limited their use in practical applications. The high losses in bends are due to the low refractive index contrast between the polymer and its surroundings. The smallest bend radius that still exhibits sufficiently low losses is in the order of tens of microns. Because of the otherwise promising properties of polymer waveguides, a practical way to reduce their bend losses is highly desirable.

Several mechanisms contribute to losses in waveguide bends: straight-to-bend and bend-to-bend mode transition losses, propagation losses, and losses due to radiation into the substrate or cladding. Pure bend losses are defined as the sum of propagation and radiation loss. With numerical simulations the Optical Sciences group at the University of Twente proved that adding a thin metal layer underneath the core of a polymer waveguide results in better confinement of the bend mode, and therefore decreases the bend losses for both polarizations. By the introduction of this metal layer the optimum radius of curvature was reduced to only a few microns.

In this work, the performance of fabricated waveguides with a metallic layer underneath (metallic waveguides) was characterized in comparison to their dielectric counterparts. TE-polarized light from a laser diode emitting at 1550 nm was coupled to the waveguides by focusing on the entrance face of the waveguides, and the output power was measured. From in- and output power measurements the total system loss was calculated. Indeed, the total system losses in sharply bent metallic waveguides with radius of curvature $R = 4$ and $R = 7$ μm were significantly lower than in the non-metallic waveguides.

The output power was measured for identical waveguides with increasing number of 90° bends. The increase in loss per two extra bends was equal to the sum of two total bend losses plus one bend-to-bend loss. Even though many of the waveguides were damaged and demonstrated unexpected extra losses, still the metallic waveguides exhibited much lower losses than the non-metallic ones. However, the obtained loss factors were 2 to 10 times smaller than was predicted by numerical simulations. It is expected that this was due to differences in thickness and width between the fabricated waveguides and the simulated structure.

Further research may focus on the determination of the pure contribution of total bend loss, by characterizing waveguides that are corner-shaped. Also it is desirable to enhance the quality of individual waveguides for more accurate measurements. This can be done by fabricating new samples as well as polishing the rough end facets of the waveguides.

Table of contents

1 Introduction

The science of photonics studies the generation, detection and signal processing of light. The inventions of the laser and the optical fiber were crucial for the success of the field and have since led to many applications, in particular in the telecommunication industries [1]. Optical signals allow broadband transmission and therefore higher information rates can be achieved [2]. For a long time it remained unknown how to guide a signal over long distances (meter to kilometer scale) with sufficiently low losses in a cost-effective way. At that time several signal carriers, such as microwaves and light, were still under investigation for this purpose [3]. A lot of research was done in order to characterize waveguides of many materials and geometries in order to realize efficient signal transmission. In microwave technology mainly hollow metal waveguides were developed. On the other hand dielectric rod waveguides were considered for optical communication. However, the high propagation losses in the materials remained a limiting factor for a long time.

In 1966 a major breakthrough was achieved when prof. Charles Kao demonstrated that most of the losses in glass waveguides were due to impurities in the material [†]. He suggested that low losses of 1dB/km could be achieved in a cylindrical dielectric waveguide made of very pure glass [3]. Today, glass optical fibers are widely used for high-speed data transfer [4]. They can guide a modulated laser signal for distances in excess of 100 km, without the need for repeaters [1].

1.1 Waveguide technologies in integrated optics

Dielectric optical fibers consist of a rod of dielectric material in which the light is confined by the principle of total internal reflection, even when the fiber is curved. The light is confined inside the fiber because of the difference in refractive index between the fiber material and its surroundings (refractive index contrast). Generally a high refractive index contrast means better light confinement and less losses in bends. In order to reduce losses even more and protect the waveguide core, most waveguides are covered by a cladding, made of a material with a slightly lower refractive index than the core.

Currently there is a lot of interest in developing low-loss waveguides for light transport on a much smaller scale: micrometer-sized waveguides that can be used in many fiber-optic applications, such as optical sensors, fiber-optic gyroscopes, variable delay lines, optical buffers for packet switching, opto-electronic oscillators, and narrow-band filters [1]. In such cases

[†]Prof. Kao was awarded half of the Nobel Prize in Physics in 2009 "for groundbreaking achievements concerning the transmission of light in fibers for optical communication". The other half was awarded jointly to Willard S. Boyle and George E. Smith "for the invention of an imaging semiconductor circuit - the CCD sensor".

waveguides are mostly used as passive elements that connect the active elements of the device, like routers, filters, amplifiers, modulators, switches, etc [4]. They can also be used as active elements (e.g. as delay lines) in sensing systems. In practice all system components often need to be placed on the same chip, in order to reduce the footprint and power consumption of the device. Such integrated optical systems are increasingly being used in sensors and telecommunication applications. Glass fibers are inconvenient for this kind of high density circuitry: they are bulky, and glass fiber devices are comparatively hard to process and expensive. Therefore many integrated photonic devices are based on new materials, such as polymers [1].

New waveguide technologies must meet economic criteria as well as technical requirements. They have to be easy to fabricate, stable under ambient conditions, compatible with other devices and efficient (i.e. low losses) [4]. In waveguide optics many different kinds of losses occur. In long, straight waveguides the dominant loss mechanism is propagation loss, which consists of intrinsic loss caused by light absorption of the material structure itself, extrinsic loss due to impurity ions left in the material, and Rayleigh loss due to the scattering of photons by the non-uniformity of the material structure [3]. However, in the pursuit of smaller and smaller integrated optical devices, waveguides exhibit more and tighter bends, which increases the contribution of bend losses. In a bent waveguide the light can partially leak into the surrounding material: the waveguide cladding or substrate. Also straight-to-bend and bend-to-bend transition losses occur because of the mode mismatch between straight and bent parts [5, 6]. Waveguides with a higher refractive index contrast between the waveguide and its surroundings and a larger radius of curvature of the bend are known to exhibit lower bend losses [7].

1.2 Waveguide materials

Plasmonic waveguides have been proposed as a promising candidate for highly integrated optical devices, because of the strong light confinement that can be achieved. In plasmonic waveguides light couples to oscillations of free electrons in a metal, which enables very tight confinement. This light waves are then called Surface Plasmon Polaritons (SPPs) [8]. The main drawback of plasmonic waveguides is the high losses that occur, due to the highly absorptive nature of metals at telecom wavelengths (1200 to 1700 nm). The trade-off between confinement and propagation losses has until now limited the application of plasmonic waveguides.

Polymer waveguides usually exhibit a low refractive index contrast, but they can be easily fabricated at low costs (thus permitting mass production) and they are robust [4, 9]. Furthermore, polymer materials span a wide range of refractive index values and exhibit a large transparency window . They are therefore compatible with many photonic technologies. Also, the optical properties of polymers can be tuned by adding dopants [9, 10]. However, due to the low refractive index contrast the bend losses in polymer waveguides are relatively high. Low-loss propagation in polymer waveguides is only possible if the radius of curvature of the waveguide is sufficiently large (typically a few tens of microns). Because of the other favourable properties of polymer waveguides, a practical way to reduce their bend losses is highly desirable.

1.3 Aim of this thesis

Recently it was shown by the Optical Sciences group at the University of Twente that embodying a thin metal layer underneath the core of a bent polymer waveguide significantly reduces the bend losses [9]. With numerical simulations it was demonstrated that the introduction of the metal reduced the optimum radius of curvature from tens of micrometers to less than 10 micrometer. These results would enable the utilization of polymer waveguides in highly integrated optical circuits and in devices where very sharp bends are necessary.

The focus of this thesis is on the experimental investigation of the properties of this new waveguide architecture. Two types of polymer waveguides were fabricated according to the proposed design: waveguides with a thin metal layer underneath and their non-metallic counterparts. The aim of the experiments is to observe whether the added metal layer enhances the waveguide performance.

The first chapter of this thesis deals with the physical principles that apply to waveguide technology in general, and more specifically with the phenomenon of losses in waveguide bends. In the next chapter, the waveguide design and simulation results of Sefunc et. al. [9] will be discussed in more detail. The details of the waveguide fabrication, the experimental setup and the characterization results are presented and discussed in chapter 4 and 5. Finally, this leads to the conclusions that are explained in chapter 6.

2 Physics of waveguides

In order to understand the principles that cause losses in waveguides, some basic knowledge about light propagation in waveguides is required. Although bend losses are of particular interest in this experiment, also other loss mechanisms play a role. The physical cause of these losses will be considered in this chapter as well. This will make it easier to accurately distinguish the contribution of bend losses and other losses at a later stage.

The simplest approach is to explain the propagation of light in waveguides is to take the point of view of geometrical optics. In geometrical optics light is considered to consist of rays that propagate in a certain direction and can be reflected or refracted at surfaces. In reality, what propagates are the wavefronts of the electromagnetic wave. The wavefronts interact with each other when they overlap: interference occurs. The effects that are involved with this interaction can be best described from the point of view of wave optics. This interpretation of the interaction between light and matter is based on the wave equation of light that can be derived from Maxwell's equations. Both approaches will be employed in this chapter.

2.1 Light propagation in dielectric waveguides

Light propagation in dielectric waveguides is based on the phenomenon of total internal reflection: light that is incident on the interface between two media can, under certain conditions, be reflected internally without losses instead of being (partially) refracted into the outside material, as shown in Fig. 2.1 [2].

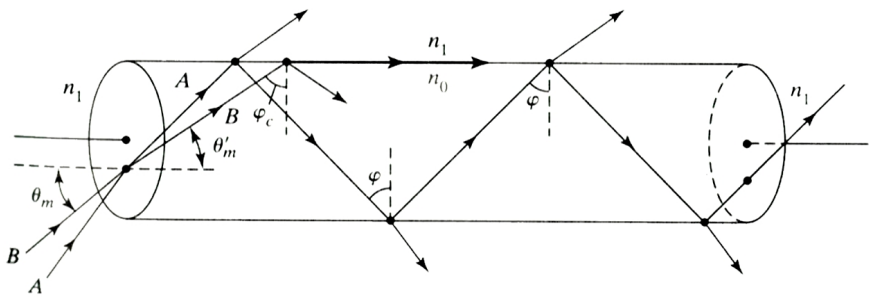

Figure 2.1: Light propagation in fiber-like waveguides enabled by total internal reflection [2]. Two light rays propagate in the cylinder waveguide. The first one, denoted with A, is only partially reflected and therefore losses occur at the interface of the two materials. Ray B is incident on the waveguide-cladding interface under the critical angle ϕ_c.

The principle of internal reflection is predicted by Maxwell's equations and can be derived from Snell's law as well. For now, only the outcome matters: total internal reflection only occurs if the angle of incidence ϕ is less than the critical angle ϕ_c, or $\phi < \phi_c = \sin^{-1}(n_1/n_0)$, with n_0 and n_1 the indices of refraction of the waveguide medium and the surronding medium or cladding, respectively (see Fig. 2.1) [2].
As a result of this relationship, total internal reflection only occurs when the refractive index of the inside medium is higher than the outside. One of the most famous applications of this principle is the transmission of optical signals through dielectric fibers.

The light gathering ability of a fiber is defined by its numerical aperture (N.A.) [2]:

$$N.A. \equiv n_0 \sin\theta_m \tag{2.1}$$

The numerical aperture thus depends on the maximum angle of incidence on the fiber entrance at which light rays can still propagate inside the fiber by means of total internal reflection. In other words, the numerical aperture gives the size of the acceptance cone of the fiber. Snell's law of refraction and the geometrical relation between θ_m and ϕ can be used to get an analytical expression for the numerical aperture, as long as the entrance face of the waveguide is flat [2].

$$N.A. \equiv n_0 \sin\theta_m = n_1 \cos\phi_c = \sqrt{n_1^2 - n_0^2} \tag{2.2}$$

2.2 Allowed modes

For successful propagation throughout the fiber some additional conditions have to be fulfilled. Because of these restrictions, only a limited number of modes is allowed in the waveguide. The reason for that can be best understood in the simpler case of a planar or slab waveguide. As shown in Fig. 2.2, each ray represents plane waves moving along the direction of the ray. Such waves overlap and interfere with one another. The reflected wave travels in its initial direction again. The twice reflected wave interferes with the original wave in a way that can be either constructive or destructive, depending on the optical path length between the two waves. If the optical path length equals a multiple of the wavelength λ, the condition of constructive interference is fulfilled and the light can propagate properly. The parameters that determine which modes can propagate, are the incoming angle, the wavelength and the diameter (more generally: geometry) of the waveguide.

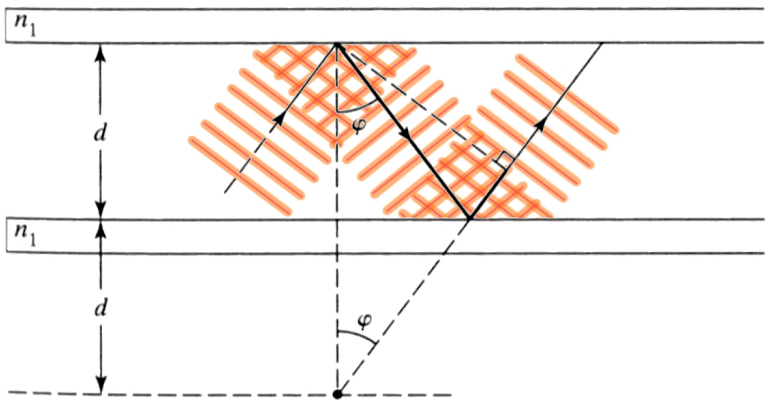

Figure 2.2: Schematic view of interference of reflected waves in a straight waveguide, based on [2]

Based on the physical principles explained above it is possible to obtain an expression for the maximum mode number. However, in the case of a cylindrical fiber this analysis is complicated and will not be carried out here. It can be shown that the maximum mode number m is the largest integer that is less than the parameter m_{max}, which is given by [2]:

$$m_{max} = \frac{1}{2}\left(\frac{\pi d}{\lambda} N.A.\right) \tag{2.3}$$

It turns out that a single-mode (or monomode) fiber can be obtained when [2]

$$\frac{d}{\lambda} < \frac{2.4}{\pi(N.A.)} \tag{2.4}$$

From the wave-optics point of view, the distribution of the magnetic and electric fields is limited by the boundary conditions that are imposed by the interface between the waveguide and the cladding. Fig. 2.3 [11] shows the spatial distribution of the electric field of some modes that are allowed in a straight waveguide. The spatial distribution of the fields is called the mode profile. Most of the time this profile is displayed as the distribution of the electric field strength throughout the cross section of the waveguide.

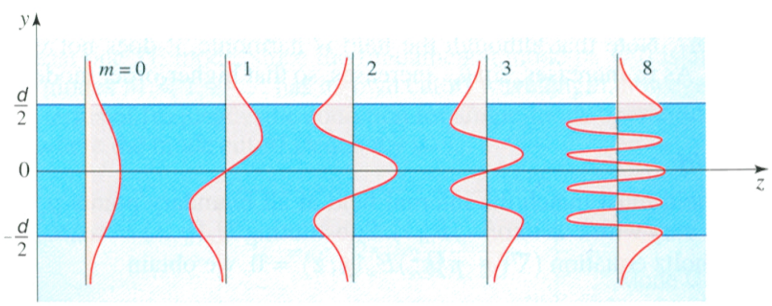

Figure 2.3: Schematic field distributions for TE guided modes in a dielectric waveguide [11]

2.3 Loss mechanisms in straight waveguides

The intensity of light propagating through the waveguide will gradually attenuate due to several loss mechanisms. Sharp bends or microbends belong to the geometric design of the waveguide, but they cause radiation loss if the condition for total internal reflection is no longer satisfied. Also in- and out-coupling losses are present due to the restrictions of the numerical aperture, and Fresnel losses occur due to reflections at the input interface. The radiation pattern and size of the light source might be ill-adapted to the fiber end, leading to radiation losses because of the mode mismatch. Other losses are caused by inhomogeneities in the waveguide itself or at the surface, typically when their dimensions are much greater than the wavelength. In addition, many other effects can cause losses when waveguides are connected to each other or to an optical device, e.g. mismatch of coupled fiber ends, separation and incompatibility of numerical apertures [2].

Intrinsic losses are caused by absorption and by Raileigh scattering. Absorption is highly wavelength selective. Which wavelengths are absorbed depends on the electronic and molecular transition bands of the waveguide material, but impurities that were left during the material processing are responsible for a great part of the absorption as well. For example in glass waveguides the hydroxyl (OH) ion significantly absorbs at wavelengths of 0.95, 1.23 and 1.73 μm [2].

2.4 Light propagation and losses in waveguide bends

The best way to understand the radiation losses that occur in bends is to keep in mind the geometrical approach as introduced above. Light rays are incident on the interface of the waveguide and its surroundings (in the experiments, air was used as cladding) and reflect back into the waveguide by the principle of total internal reflection. However, when the light arrives at a bend section, the interface of the waveguide is slightly turned with respect to the direction of the light, as can be seen in Fig. 2.4(a). The light that propagates towards the outer rim of the bend will incide on interface under another angle of incidence. In sharp bends this angle may be smaller than the critical angle and the light will enter the regime of partial internal reflection. The light that is not reflected internally will radiate out of the waveguide: bend loss occurs.

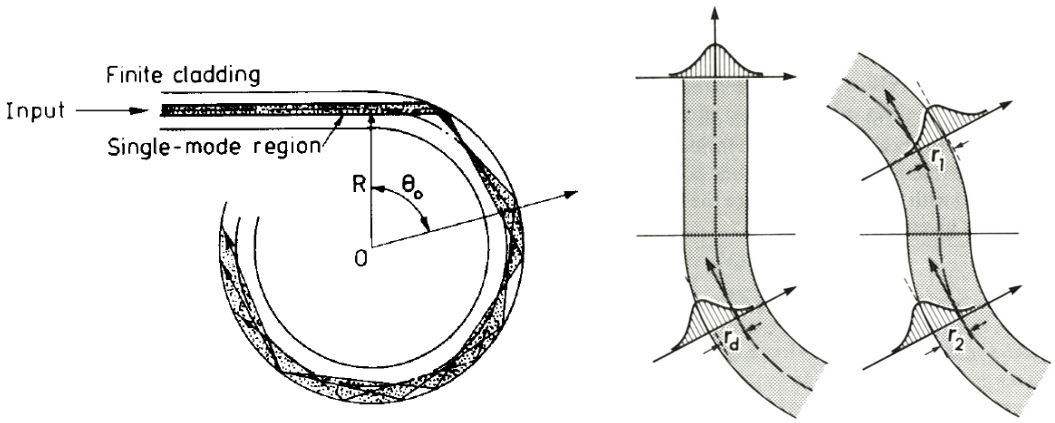

(a) Ray propagation in waveguide bends [5]

(b) Straight-to-bend and bend-to-bend mode transition [6]

Figure 2.4: Light propagation in bends represented as rays (a) and represented with the fundamental mode field distribution (b)

Although this approach serves well to explain the significantly increased propagation losses in bent waveguides, its practical use is very limited. For example the behaviour of skew rays (i.e. rays that do not propagate in the central plane) is more difficult to explain because then the 3-D geometry of the system becomes important. Discussing all other possible rays would require a much more detailed analysis. However, when it comes to calculating bend losses, usually the wave equations for light are preferred as starting point, in accordance with the common approach for examining light propagation in straight waveguides.

The radius of curvature of a bend is defined as the distance between the center of curvature and the waveguide. Often the distance is measured to the center of the waveguide, similar to the situation in Fig. 2.4.

In general, two types of curvature losses can be identified [12] (first proposed by Gambling et.al. [13]): transition loss (due to mode conversion) and pure bending loss. It has been shown that the field distribution in bends (the bend mode) differs from the straight waveguide mode. In bends most energy of the mode is located close to the outer rim of the curve (Fig. 2.4(b) [5, 7, 14]). In straight waveguides, however, the energy usually is distributed symmetrically with respect to the waveguide center (see Fig. 2.3).

Mode conversion occurs between the straight waveguide mode and the bend mode, and in that process energy is lost. This is called straight-to-bend loss. It is often assumed that a fixed amount of light is lost at the straight-to-bend 'interface'. However, in reality the mode conversion happens over the first few radians of the bend as can be seen in Fig. 2.4(a). The light is lost in discrete rays instead of uniformly, as was shown among others by W.A. Gambling et. al. in multiple experiments [5, 13, 15–17]. Mode conversion also happens when the rate of curvature changes sign (i.e. in S-shaped bends) leading to bend-to-bend transition loss. High transition losses can be prevented by gradually increasing the rate of curvature of the fiber instead of inducing an abrupt change between a straight and a bent section [5, 16].

The pure bending loss arises when the light propagates in the bend mode. Some part of the mode propagates closer to the center of curvature (e.g. at the inner rim of the waveguide) and another part propagates more far away. The light velocity increases linearly with increasing

distance from the center of curvature. If all light would be contained, at a certain distance the phase velocity would exceed the speed of light [13]. Instead, this part of the light becomes evanescent, therefore it is lost in the far field.

2.5 Loss calculations

The loss L in dB is given by the logaritm of the ratio of P_{out} and P_{in}:

$$L \equiv 10 \cdot \log_{10} \left(\frac{P_{out}}{P_{in}} \right) \tag{2.5}$$

with P_{out} the power of the output signal, and P_{in} the original input power. For integrated optical waveguides, losses are usually expressed in decibels per centimeter (dB/cm).

When a system is subject to multiple loss types, the individual losses in dB can be added to give the total system loss (TSL) in dB:

$$TSL = L_1 + L_2 + L_3 + ... \tag{2.6}$$

3 Low-loss hybrid dielectric metallic waveguides with sharp bends

The waveguide architecture considered in this study is presented in Fig. 3.1 [9]. The proposed configuration consists of a polymer channel waveguide and a thin gold layer underneath, which are separated by a buffer layer of SiO_2. The waveguide core material was chosen as SU-8, a negative-tone epoxy resist. This configuration will be referred to as 'metallic'. The same architecture but without metal layer was used for reference and will be referred to as 'non-metallic' from here on. Typical waveguide dimensions are as follows: $h_{ridge} = 2$ μm and $w_{ridge} = 2$ μm, $t_{buffer} = 100$ nm and $t_{metal} = 50$ nm. The loss reduction caused by the metal layer (as demonstrated later in this chapter) was also observed with different system geometries [9]. At the wavelength of interest $\lambda = 1550$ nm (the conventional telecom wavelength) this is a single-mode waveguide [18].

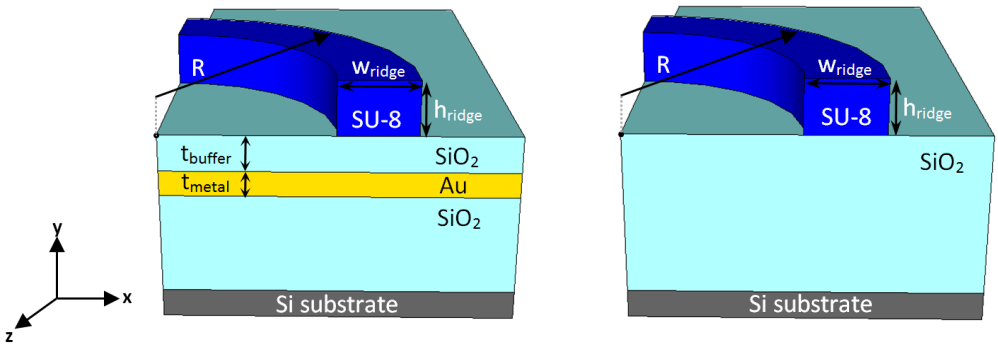

(a) Metallic configurationl (b) Non-metallic configuration

Figure 3.1: 3-D view of waveguide architectures studied in this work (reproduced from [9] with permission)

The radius of curvature is defined as the distance between the center of curvature and the outer rim of the waveguide as shown in Fig. 3.1. This definition seems appropriate because in bends, most of the energy is located close to the outer rim. The refractive indices of the materials employed in the waveguide design are presented in table 3.1.

	Material	Refractive index
Under cladding	SiO_2	1.444
Metal	Au	$0.55 + 11.5i$
Buffer	SiO_2	1.444
Waveguide	SU-8	$1.57 + 4.93 \cdot 10^{-6}i$
Upper cladding	Air	1

Table 3.1: Refractive indices of the materials employed in the waveguide design

3.1 Simulation results

With numerical simulations the propagation of light was investigated for both the metallic and non-metallic waveguides, in order to calculate the total losses per 90 degree bend [9]. The total bend loss (TBL) in dB/90° was calculated from the imaginary part of the effective refractive index of the mode, according to the equation:

$$TBL = 10 \cdot \log_{10} \left[\Im(n_{eff}) k_0 R \pi \right] \tag{3.1}$$

Here n_{eff} is the complex effective refractive index of the guided mode in the bent waveguide and k_0 is the wavenumber in vacuum ($k_0 = 2\pi/\lambda$). The total bend loss includes both the radiation loss due to the waveguide curvature (pure bending loss) as well as the propagation loss due to scattering and absorption in the SU-8 and metal layers. The finite difference (FD) mode calculations were performed in FieldDesigner software by Phoenix Software B.V.

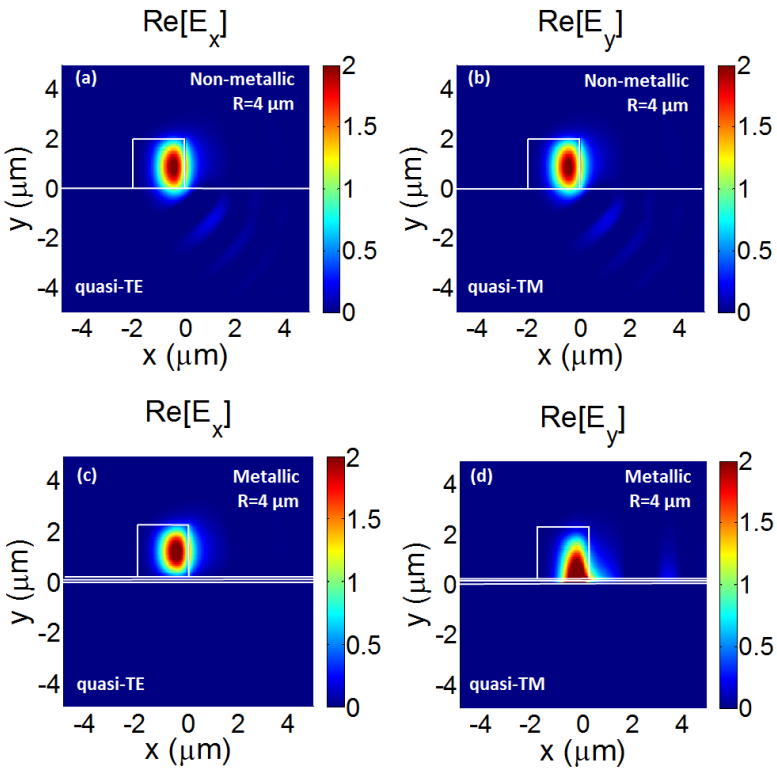

Figure 3.2: Simulated profiles of the TE and TM modes in metallic and non-metallic waveguide bends with $R = 4$ μm.

In Fig. 3.2 the calculated profiles of the bend modes are shown, for both TE (a) and TM (b) polarizations. Significant light leakage can be observed in the non-metallic modes (Fig. 3.2 (a) and (b)). The light radiates into the substrate rather than the surrounding air, due to lower refractive index contrast between the waveguide and the substrate. When a metal layer is introduced, most of the radiation can be prevented (Fig. 3.2 (c) and (d)). Radiation from the TE-polarized mode is blocked by the metal layer and the mode is pushed towards the positive y-axis direction (see Fig. 3.1). Radiation from the TM mode partially couples to the metal and is transformed into a plasmonic-photonic hybrid mode. Because of the coupling to the metal, leakage to the substrate is prevented as well.

The total bend losses per 90° bend are shown in Fig. 3.3. The bend losses in non-metallic waveguides increase with smaller values of radius of curvature R. In metallic waveguides two regimes can be identified. In the first regime, for small values of R, the advantage of having a thin metal layer is observed by reduced losses compared to the non-metallic case. When R becomes larger, the effects of absorption by the metal layer becomes dominant. When absorption effects are dominant, the bend losses increase with increased R, because total absorption losses increase linearly with the length of the waveguide.

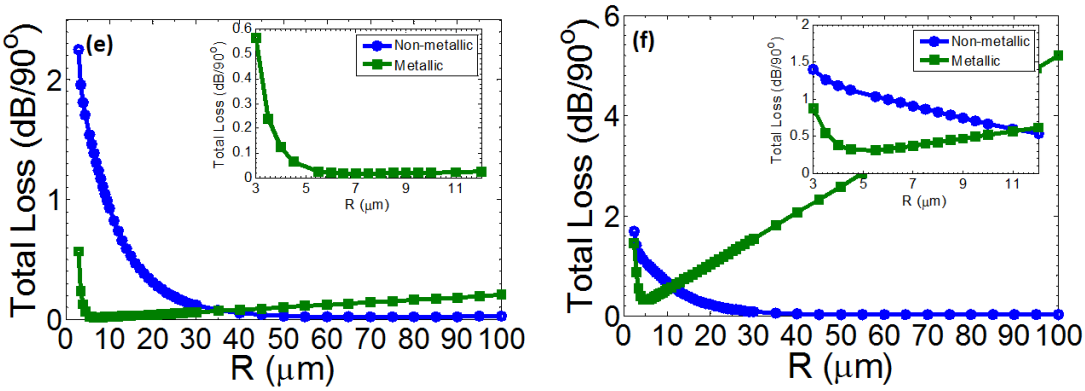

(a) TE polarization

(b) TM polarization

Figure 3.3: Total bend loss versus radius of curvature in metallic and non-metallic waveguides [9]. The insets are a zoom of the corresponding loss plot in the region of interest, i.e. where minimum losses occur.

Fig. 3.3 shows that in metallic waveguides the bend losses in sharp bends are significantly reduced for both polarizations. The introduction of the thin metal layer shifts the optimum radius from several tens of microns to less than 10 micron. The best results are obtained for TE-polarization where 0.02 dB loss per 90 degrees was obtained at the optimum radius $R = 7$ μm.

4 Characterization conditions

In a comparative study multiple metallic and non-metallic waveguides were characterized by measuring the power of the transmitted light through those waveguides at a constant input power. The aim of the experiments is to investigate the loss reduction caused by the additional metal layer. In the experiments only TE polarized light was used, because for this polarization the advantage of adding a metal layer is the most significant according to numerical simulations (as discussed in chapter 3).

4.1 Fabrication of metallic and non-metallic SU-8 waveguides

Metallic and non-metallic waveguides were fabricated with various numbers of bends to experimentally investigate the effect of the metal layer on the system losses. The waveguide design is schematically shown in Fig. 4.1. Both waveguide types were fabricated on one wafer, in one run with the same mask properties. Apart from the additional metal layer, the metallic waveguides (Fig. 4.1(b)) were identical to their non-metallic counterparts (Fig. 4.1(a)) to enable fair comparison. The waveguides were tapered at the input section to enhance the coupling efficiency in experiments.

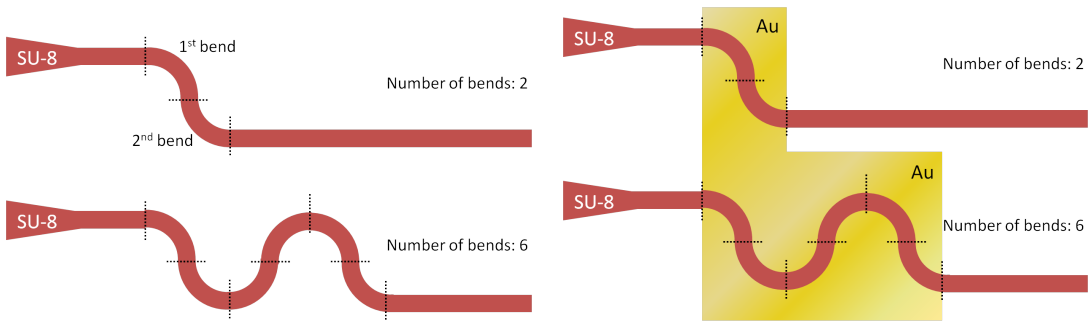

(a) Non-metallic waveguides (b) Metallic waveguides

Figure 4.1: Schematic view of fabricated metallic and non-metallic waveguides

The fabrication of the waveguides involved three main steps: patterning of the gold layer, deposition of the SiO_2 buffer layer, and patterning of the waveguides on SU-8 resist. As the substrate a standard silicon wafer was used with a pre-deposited 8 μm oxide layer on top. This layer is large enough to avoid light leakage to the Si substrate [18]. The wafer was cleaned

with the standard wafer cleaning procedure. Then a positive photoresist was spin coated on the wafer and patterned using UV-photolithography, to determine the precise shape of the gold layer. The gold is only located underneath the bend sections of the metallic waveguides. The photoresist that had been exposed to the UV-light was removed. A 50 nm gold layer was evaporated on the wafer and then with the lift-off technique the leftover positive resist was removed. Subsequently a 100 nm thick amorphous SiO_2 layer was deposited using the electron beam evaporation method. A thin layer of SU-8 negative photoresist was then spin coated on the wafer with a thickness of 2 μm. Finally, the SU-8 channel waveguides were created with 2 micron width by patterning the resist. The excess (non-exposed) SU-8 was removed after the patterning. Microscope images of the fabricated waveguides are shown in Fig. 4.2.

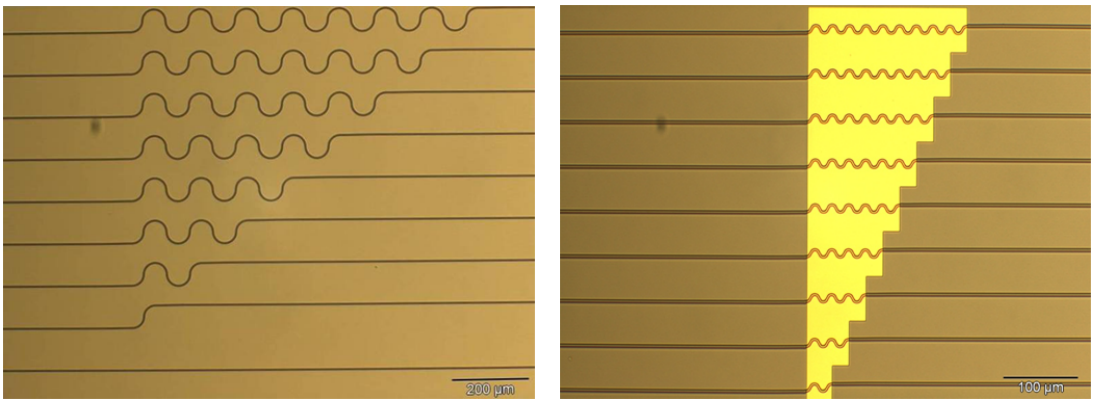

(a) Non-metallic waveguides after fabrication (b) Metallic waveguides after fabrication

Figure 4.2: Micro-images of fabricated waveguides

The wafer was diced into smaller chips that were easier to handle. In this process the waveguides were slightly cut off to create end facets that were exactly at the edge of the sample. Unfortunately the end facets of the waveguides were very rough (Fig. 4.3).

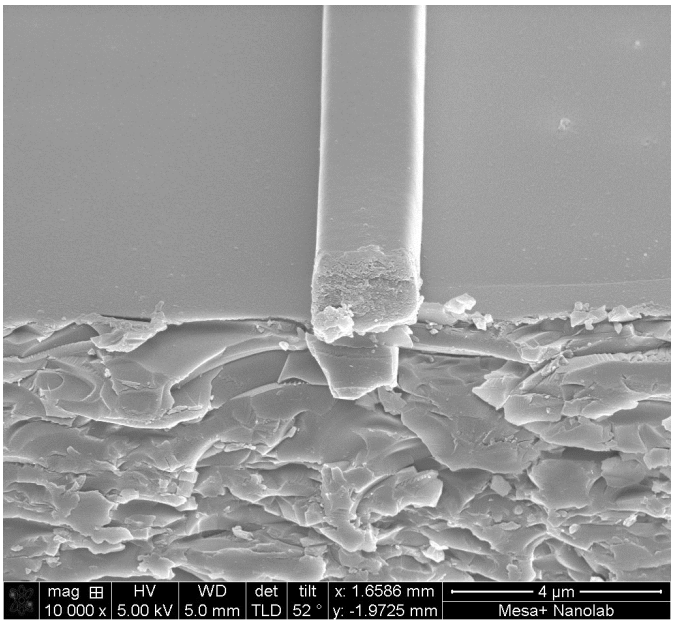

Figure 4.3: SEM image of unpolished waveguide end facet. In the upper half of the image, the channel waveguide and its end facet are visible. The under half shows the side facet of the SiO_2 substrate.

4.2 Characterization setup

The setup used for characterizing the waveguides performance is schematically shown in Fig. 4.4. As a light source a semiconductor laser diode was used that emits light at a wavelength of 1550 nm. This is one of the standard wavelengths for optical telecommunications. The light was guided towards the sample with a pigtailed polarization-maintaining (PM) fiber. The polarization was chosen as TE, because the numerical simulations suggest that the differences between metallic and non-metallic waveguides are stronger for this polarization compared to TM polarized light. The current of the laser diode and its internal temperature were kept constant with a temperature/current controller.

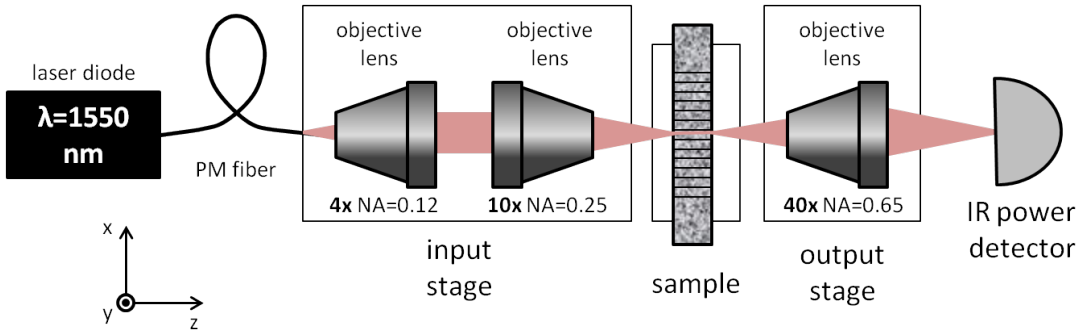

Figure 4.4: Waveguide characterization setup

The divergent beam coming from the fiber tip was collimated with an objective lens with 4x magnification. Then the light was focused to the waveguide end-facet using another objective lens with 10x magnification. This way the light coupled to the waveguide and light propagation inside the waveguide was realized. The objective lens at the output stage was used to focus the output light coming from the waveguide end facet on the infrared power detector. With a microscope the sample could be observed from above.

4.3 Coupling optimization procedure

It is hard to obtain good coupling with infrared light at once, because it is impossible to visually observe when coupling is obtained. Therefore a red light source was used to align the setup and get as close as possible to infrared coupling conditions. For this a HeNe laser (wavelength $\lambda = 632.8$ nm) was used to which a fiber was attached as well. The in- and output stage were aligned such that the red light was coupled to the waveguides as much as possible (as far as could be observed by eye). Then the light source was changed. At this time the x and y position of the in- and output stage (see Fig. 4.4) should be roughly correct already. Only the z-position of the objectives should be slightly changed, because the focus length of the objectives depends on the wavelength of the light. With an IR camera the output end facet of the waveguide was observed. This made it possible to quickly determine the correct position of both stages by maximizing the intensity of the output light at the camera display.

In order to measure the output power of the waveguide, the IR camera is replaced with a power detector. At each single measurement the x, y and z position of the input and output

stages were carefully adjusted until the output power was maximized. This indicates that the best possible coupling to the waveguide was obtained. The optimization procedure enabled reliable measurements that were reproducible within an error margin of 10%.

4.4 Analysis

The aim of this study was to measure the total bend losses. This relates to the total of propagation and radiation losses that occur in the waveguide bends. In the experiments the output power was measured at the end of the waveguide and compared with the input power. The total system loss (TSL) in dB was calculated according to:

$$TSL = 10 \cdot \log_{10}(P_{out}/P_{in}) \tag{4.1}$$

where P_{in} is the input power and P_{out} the output power in Watt.

However, in the sample configuration that was used, other losses play a role as well. Fig. 4.5 shows schematically at what parts of the fabricated waveguides the mentioned loss types arise. The physical principles that cause these losses have already been discussed in chapter 2. In this section their expected contribution to the total system loss will be discussed.

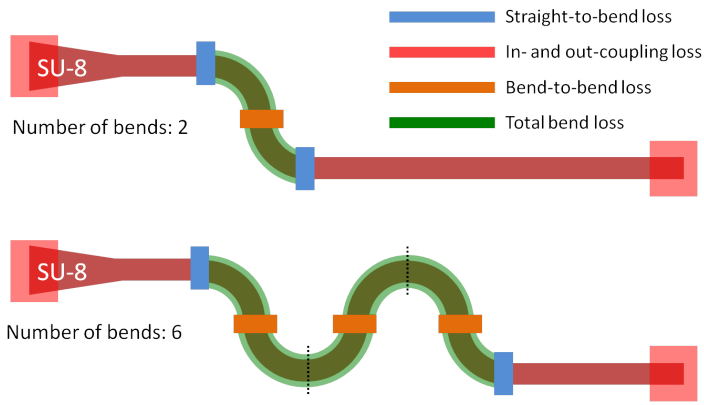

Figure 4.5: Schematic representation of loss types in the waveguides.

- **In-coupling losses due to the mode mismatch between the fiber and the waveguide**
  The in-coupling losses of the waveguides may vary, because of the bad end-facet quality. This influences the acceptance cone of the waveguide in an unpredictable way. If the end-facets of the waveguides had been flat, the in-coupling loss would be equal for all waveguides. Unfortunately for the used samples this was not the case, and it is assumed that the in-coupling loss varies among waveguides. The same holds for the out-coupling loss.

- **Straight-to-bend transition losses**
  The straight-to-bend transition loss occurs only at the beginning and at the end of the bent section. The contribution of this loss type is equal for all waveguides.

- **Bend-to-bend transition losses**
  Bend-to-bend transition losses (BtB) are present at any part of the waveguide where the

direction of curvature switches, like in S-bends. The contribution of bend-to-bend losses relative to the total bend loss increases with smaller values of the radius of curvature R.

- **Propagation losses in the straight part of the waveguides**
  The propagation losses in the straight sections are approximately equal for all waveguides. This is because in reality the straight sections are much longer than the bent sections. Besides, the contribution of the propagation loss is relatively small compared to that of the bend losses: only 0.17 dB/mm was measured by Yang et. al [18].

- **Losses in the imaging part of the setup ('out-coupling losses')**
  The out-coupling losses are approximately equal to the in-coupling losses.

Fig. 4.5 also shows that with increasing the number of bends in the structure, only of several loss types the contribution is increased. In a waveguide with 2 bends, the total system loss is the sum of the in- and out-coupling loss, 2*propagation loss, 2*straight-to-bend transition loss, 1*bend-to-bend transition loss, and 2*total bend loss. In a waveguide with 6 bends, the total system loss is given by the sum of in- and out-coupling loss, 2*propagation loss, 2*straight-to-bend transition loss, 3*bend-to-bend transition loss, and 6*total bend loss.

In general, the total system loss TSL in dB can be described with

$$TSL = offset + \frac{N}{2}(2 \cdot BL + BtB) \tag{4.2}$$

with $offset$ = in- and outcoupling loss + 2*propagation loss + 2*straight-to-bend transition loss in dB, N the number of bends in the waveguide, BL the total bend loss in dB, and BtB the bend-to-bend transition loss in dB.

When the total system loss is plotted versus $N/2$, the slope α of the curve will represent the sum of 2*total bend loss (BL) in dB plus 1*bend-to-bend transition loss (BtB) in dB[†]:

$$\alpha = 2 \cdot BL + BtB \tag{4.3}$$

Mode-overlap calculations predicted that for the characterized waveguide sets, with $R = 4$ and $R = 7$ μm, the bend-to-bend losses dominate compared to the contribution of the total bend loss, as shown in table 4.1.

Waveguide design	**Total bend loss**	**BtB transition loss**
Non-metallic, $R = 7$ μm	1.31 dB	5.26 dB
Metallic, $R = 7$ μm	0.017 dB	4.21 dB
Non-metallic, $R = 4$ μm	1.8 dB	10.3 dB
Metallic, $R = 4$ μm	0.12 dB	9.6 dB

Table 4.1: Numerical simulation results for the total bend loss (TBL) and bend-to-bend transition loss (BtB) in waveguides with $R = 7$ μm and $R = 4$ μm

[†]At first hand it seems more straightforward to plot the bend loss versus the number of bends, without dividing by two. In that case the slope of the curve would equal 1*total bend loss + 1/2*bend-to-bend loss. This approach, however, would suggest that for each extra bend the contribution of the bend-to-bend loss increases. In reality this is not the case: an extra bend-to-bend loss can *only* occur when two extra bends are added in the waveguide. Therefore it was chosen to present the data such that the slope of the curve equals the loss per two 90° bends.

5 Characterization results

In this chapter the characterization results are presented. First of all, a series of measurements was performed that enabled the calculation of the statistical error (defined as the 99% confidence interval) in the input power measurements. After that the output power was measured for metallic and non-metallic waveguides with $R = 7$ and $R = 4$ μm. The experimental results are discussed and it is suggested how further research could be performed.

5.1 Input power stability and output power error

The input power was measured right after the objectives on the input stage. The diode temperature and current were kept constant at 21.60 °C and 35.42 mA, respectively. The input power stability was measured by attaching and removing the fiber tip multiple times. The changes in the fiber curvature might fluctuate the fiber power. From a series of 13 measurements it was calculated that the input power was stable at the interval of 0.895 ± 0.004 mW. The error margin of the input power is approximately 0.5%. The dimensions of the confidence interval were determined with the method presented in [19]. The output power depends linearly on input power. Therefore the probable error in output power due to input power variation is expected to be 0.5% as well.

5.2 Waveguide quality

The quality of the waveguides was investigated by measuring the output power of 38 straight waveguides, at a constant input power. According to the wafer design, all straight waveguides should be identical, and therefore similar values for the output power were expected. However, from the experiments it was observed that the output power values were ranging from 10 to 100 microwatt at constant input power of 0.895 ± 0.004 mW. The measured values are presented in a histogram in Fig. 5.1.

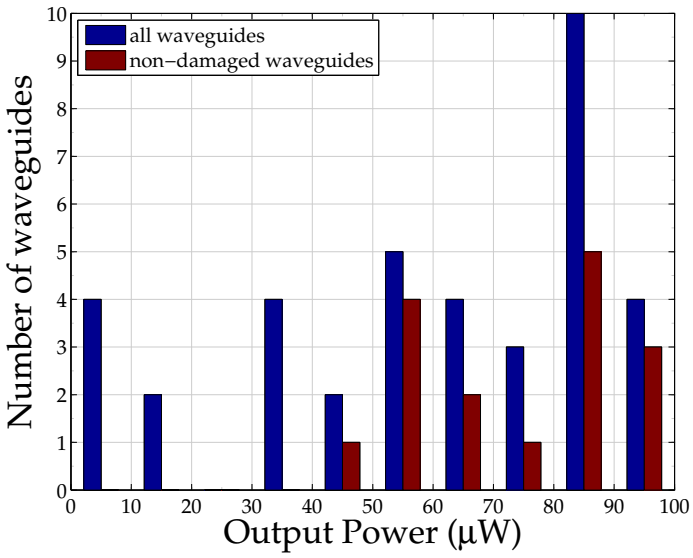

Figure 5.1: Histogram of waveguide output power measurements. The height of each bar represents the number of waveguides that had an output power in the corresponding interval specified on the x-axis. The histogram indicated with 'all waveguides' was based on output power measurements of 38 straight waveguides. From these, only 16 waveguides were not visibly damaged. The output power measurements of these 'non-damaged' waveguides were presented separately.

The measurements themselves were well reproducible, as will be demonstrated later. Therefore this unexpected result must be due to factors that influence the quality of individual waveguides. As discussed before, the end facets of the waveguides were very rough. This leads to an unpredictable increase in in- and out-coupling losses which may be different for each waveguide. Additionally, the propagation loss includes losses due to sidewall roughness and scattering at defects. Indeed, with the microscope in some waveguides bright scattering points could be observed when light propagated inside. These inhomogeneities could originate from the fabrication process as well as human errors during the experiments. The handling of the chips was quite hard and they have been dropped accidentally during the experiments. It is thus very likely that the uncladded waveguides were damaged during the experimental phase as well. Altogether, these observations indicate that the waveguides were of low quality and that individual waveguides were severely damaged.

It is possible to identify the most badly damaged waveguides by eye. However, the red bars in Fig. 5.1 show that even when these waveguides are left out of consideration, the output power still is not stable at all (variation is more than 50% of the maximum value). It turns out it is hardly possible to discriminate between undamaged ('healthy') and damaged waveguides.

5.3 Measurement reproducibility

From microscope observations it was decided to characterize the waveguide sets with radius of curvature $R = 4$ and $R = 7$ μm, because these sets seemed to exhibit the least defects. The set with $R = 7$ μm is especially interesting because, according to the simulations, this is the

optimum radius of curvature for the metallic TE mode.

In order to test the robustness of the coupling optimization procedure, the characterization of the metallic and non-metallic waveguides with $R = 7$ μm was repeated twice. Afterwards, the 99% confidence interval of the average value was estimated. The results are presented in Fig. 5.2.

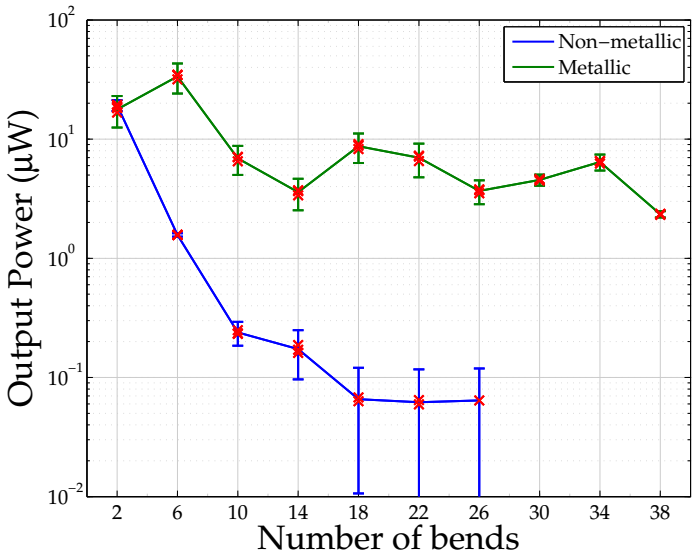

Figure 5.2: Repeated measurements of the output power of waveguides with R = 7 μm and varying numbers of bends. The input power was constant at 895 ± 0.05 *μW. The solid curves represent the average output power. The red crosses indicate individual measurements, and the error bars define the size of the 99% confidence interval*

The size of the error bars was calculated similar to the error in the input power, following the method proposed by [19]. The error bars are relatively large because there were only three or less data points per waveguide. This increases the statistical error significantly. However, it is clear that multiple measurements are in good agreement with each other. The standard deviation of the data points per waveguide was 7% of the average at most.

5.4 Characterization results of waveguides with $R = 7$ and $R = 4$ μm

From the results presented in Fig. 5.2 it can be observed that the output power of both waveguide designs decreases significantly with increasing number of bends. This was expected since the total radiation in bends and the total bend-to-bend transition loss in the system increases with increasing number of bends. In the non-metallic waveguides the output power quickly decreased into noise level (approximately 0.06 μW). Therefore no measurements were taken for non-metallic waveguides with more than 26 bends. The output power of the metallic waveguides shows a lot of fluctuations. These are most likely related to the individual waveguide quality. As argued earlier in this section, waveguide damages may reduce the output power by more than 50%.

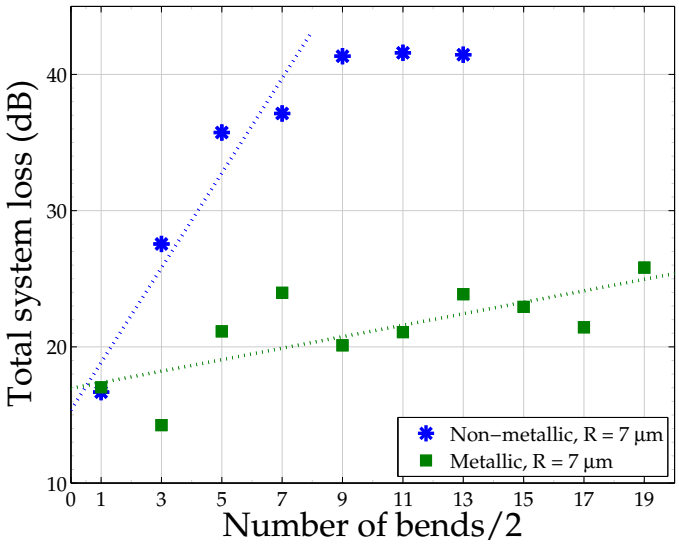

Figure 5.3: Total system loss versus number of bends divided by 2 in metallic and non-metallic waveguides. The radius of curvature of the bends was 7 µm. The input power was 895 ± 5 µW and the light was TE-polarized.

The total system losses, as defined in Eq. 4.2, are presented in Fig. 5.3. On the x-axis, the number of bends divided by two is given. A linear fit was added in order to obtain an approximate value for the loss increase per two added bend. It was proposed in section 4.4 that the slope of the curve should be equal to 2 times the total bend loss plus one bend-to-bend transition loss. The obtained slope and the theoretical prediction are shown in table 5.1

Waveguide design	**2*TBL + BtB**	**Experimental slope**	**Difference factor**
Non-metallic	7.88 dB	3.46 dB	2.3
Metallic	4.24 dB	0.42 dB	10.1

Table 5.1: Theoretical predictions for the total bend loss (TBL) and bend-to-bend transition loss (BtB) in waveguides with $R = 7$ µm in comparison with experimentally determined slope

The measured losses per two bends were significantly smaller than the numerically predicted values. A similar effect occured in the experimental results for waveguides with $R = 4$ µm, shown in Fig. 5.4 and table 5.2

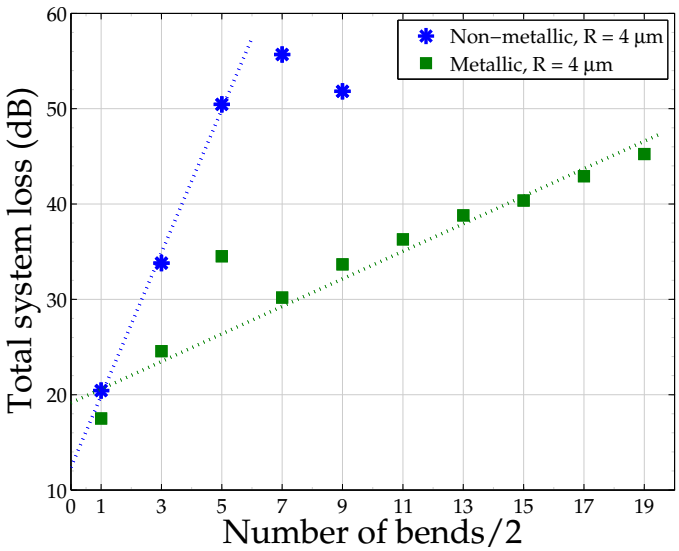

Figure 5.4: Total system loss versus number of bends divided by 2 in metallic and non-metallic waveguides. The radius of curvature of the bends was 4 µm. The input power was 895± 5 µW and the light was TE-polarized.

The output power measurements of the waveguides with $R = 4$ μm were taken under the same conditions as the $R = 7$ μm experiments. This time the output power values did not fluctuate as much as in the previous experiment with the $R = 7$ μm waveguides. Possibly the waveguides used in this experiment were less damaged than the set with $R = 7$ μm. From the output power measurements, the total system loss was calculated and plotted in Fig. 5.4. Again, a linear fit was added to the data. The data points in the noise regime were not considered in this fit.

The losses per bend were expected to be higher than in bends with $R = 7$ μm, because at $R = 7$ μm a minimum in bend losses was predicted. The experiments show that the losses per bend are indeed higher in waveguides with $R = 4$ μm compared to those with $R = 7$ μm. However, the losses are still much lower than expected.

Waveguide design	2*TBL + BtB	Experimental slope	Difference factor
Non-metallic	13.9 dB	7.0 dB	2.0
Metallic	9.84 dB	1.64 dB	6.0

Table 5.2: Theoretical predictions for the total bend loss (TBL) and bend-to-bend transition loss (BtB) in waveguides with R = 4 µm in comparison with experimentally determined slope

5.5 Discussion

The experimental results for 2*bend-to-bend transition loss + 1*total bend loss were significantly lower than the simulation results. From multiple output power measurements of the $R = 7$ μm waveguides (presented in Fig. 5.2) it is obvious that the followed procedure gives very reliable results that are well reproducible. Furthermore, a systematic error in the in- or output measurements would influence all measurements equally and would not add to the loss per two extra bends. The most likely explanation for the unexpected loss decrease is that it is caused by differences in structure between the simulated and the fabricated waveguides.

Waveguide design	Difference factor
Non-metallic, $R = 7$ μm	2.3
Metallic, $R = 7$ μm	10.1
Non-metallic, $R = 4$ μm	2.0
Metallic, $R = 4$ μm	6.0

*Table 5.3: Difference factor between experimental and simulation results for 2*TBL + BtB in metallic and non-metallic waveguides with $R = 7$ and $R = 4$ μm*

Table 5.3 shows the difference factor between the experimental and the simulated values. For both radii of curvature, the difference in performance with the expected results is the highest for metallic waveguides. Also the results for waveguides with higher radius of curvature ($R = 7$ μm) diverge more from the expected behaviour when compared to waveguides with the same configuration but $R = 4$ μm.

The first possible explanation comes from the spin-coating process of the SU-8 on the wafer. The parameters in this process were optimized for a layer thickness of 2 μm at the center of the wafer. It was estimated that the layer could be up to 10% thinner towards the outside. The characterized waveguides were part of a chip that was patterned relatively close to the wafer edge. Therefore the fabricated waveguides might be thinner than the 2 μm that was simulated.

Besides, it seems likely that the limitations of the photolithography process have caused two more differences between the simulated and the fabricated structure. The shape of waveguides fabricated from a negative photoresist was rather trapezoidal than square. In other words, the width of the waveguide at its top surface is smaller than at the bottom. When the waveguide is narrower, there will be more overlap between the bend modes in different bend directions. With numerical mode overlap simulations it was shown that the effect on the bend-to-bend transition loss of decreasing the upper width by 0.2 μm was a loss decrease of approximately 20% in metallic waveguides.

Another effect that was observed from microscope images of the waveguides is that the waveguides were narrower in sections that were patterned on the SiO_2 with a gold layer underneath (see Fig. 5.5). This is due to higher absorption and lower reflectivity of the gold layer for UV wavelengths with respect to the SiO_2. Usually during exposure of the SU-8, the light reflected by the substrate contributes to cross-linking of the polymers, which increases the waveguide size. On top of the gold layer the reflectivity is less and therefore the waveguides are narrower. The estimated difference in width is approximately 10%.

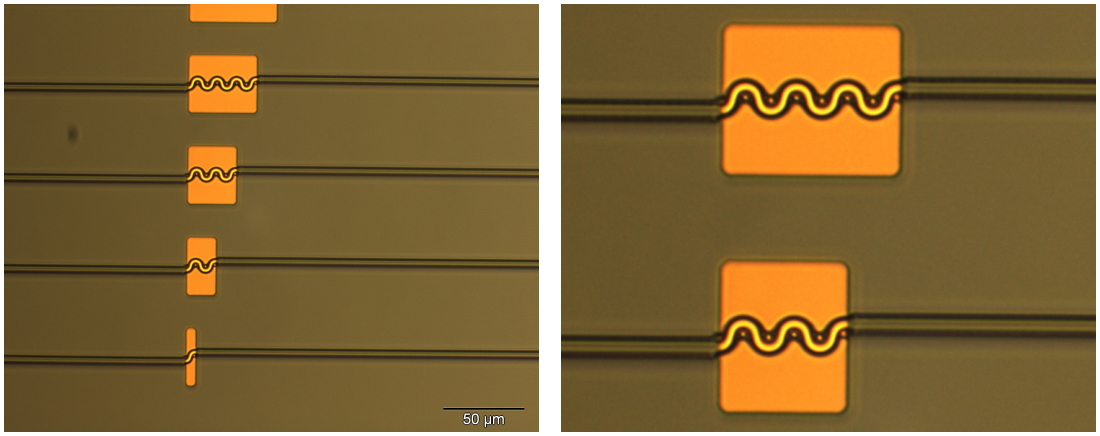

(a) Waveguides with gold layer underneath (b) Enlargement of the metallic section

Figure 5.5: Microscope image of fabricated waveguides. The enlargement of the photo (b) shows the difference in waveguide width between the sections patterned on the gold layer and only the SiO_2 substrate.

In general the bend-to-bend mode overlap will increase when the waveguides become thinner and narrower, thus lowering the bend-to-bend transition loss. Because the calculated losses were clearly dominated by bend-to-bend transition losses, the smaller waveguide size might have caused the significant loss decrease that was observed in the experiments. The differences in waveguide width between the metallic and non-metallic bend sections may be the cause of the even higher loss reduction in the metallic waveguides. However, this does not tell why the results for waveguides with $R = 7$ μm are closer to the simulations compared to $R = 4$ μm. Further simulations and investigation of the characterized waveguide structures are needed to explain the experimental results with more certainty.

5.6 Suggested approach for the determination of the total bend loss contribution

The waveguide design that was used in these experiments does not allow to distinguish between the contributions of the total bend loss and the bend-to-bend transition loss to the system losses. However, further investigation of the two contributions is interesting for two reasons. First of all, the results of such experiments can be better compared to the numerical simulations that calculated only the total bend loss. Secondly, a quantitative study of both contributions could reveal which of these loss types was most affected by the unexpected loss reduction that was observed.

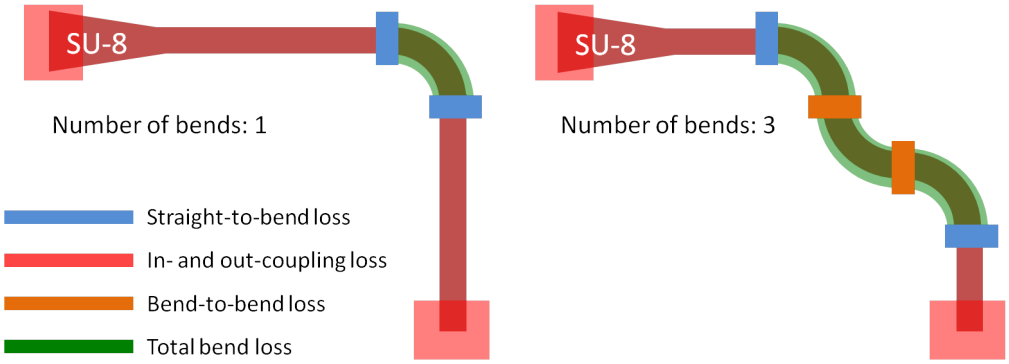

Figure 5.6: Non-metallic and metallic corner waveguides

In Fig. 5.6 another waveguide design is proposed that exhibits a different relationship between the number of bends and the contributions of loss types. The waveguides in this configuration are called 'corner waveguides' for convenience. The basic structure has one bend, and the total system losses consist of in- and out-coupling losses, two times propagation losses, two times straight-to-bend transition losses and one total bend loss. Each subsequent waveguide can contain two more bends. Each increase of two bends leads to an increase in losses equal to 2*total bend loss and 2*bend-to-bend transition loss.

If again the total system losses would be plotted against the number of bends divided by two, the slope of the curve thus equals 2*total bend loss and 2*bend-to-bend transition losses. Together with the experiments that were already performed, this forms a system with two independent equations with the unknown variables TBL and BtB that can be solved to obtain TBL and BtB.

6 Conclusion

The reduction of bend losses induced by a thin metal layer underneath polymer waveguide bends was experimentally confirmed for TE-polarized light. The total system losses in sharply bent metallic waveguides with $R = 4$ μm and $R = 7$ μm (presented in Fig. 5.4 and 5.3) were significantly lower than in their non-metallic counterparts. With these results it is proven that adding the metal layer indeed enhances the waveguides' performance.

A comparative study of losses in identical straight waveguides leads to the conclusion that a better sample quality is desired. At a constant input power, the output power fluctuated among individual waveguides by more than 50 % of the maximum measured value. The cause of this could be light that scatters at defects, or less in-coupling power because of the rough end facets of the waveguides. Partially, these defects can be due to the fabrication process, but handling the waveguide samples during experiments may have damaged them as well. The waveguides were quite vulnerable for damages because they were non-cladded and the SU-8 material is relatively soft. The bad sample quality showed up again in the output measurements of bent waveguides with $R = 7$ μm, where it is supposed to have caused unexpected extra losses that resulted in a bumpy instead of a flat curve.

Waveguide design	**2*TBL + BtB, simulation results**	**2*TBL + BtB, experimental results**
Non-metallic, R = 7 μm	7.88 dB	3.46 dB
Metallic, R = 7 μm	4.24 dB	0.42 dB
Non-metallic, R = 4 μm	13.9 dB	7.0 dB
Metallic, R=4 μm	9.84 dB	1.64 dB

Table 6.1: Theoretical predictions for the total bend loss (TBL) and bend-to-bend transition loss (BtB) in waveguides with R = 4 μm and R = 7 μm, in comparison with experimental values

The wafer design allowed measurements of the output power of the waveguides for an increasing number of bends. The loss increase at an increasing number of bends consists of contributions from total bend loss and bend-to-bend transition loss. The obtained values are presented in table 6.1. Despite the bad waveguide quality, the increase in system loss per two extra bends was much smaller than expected. The experimental values for 2*total bend losses plus 1*bend-to-bend transition loss differed from the values predicted by simulations by roughly a factor 2 to 10. The most likely explanation of this result is that the fabricated waveguides were slightly thinner and the upper surface was narrower than in the simulated structure. Also the waveguides that were patterned above the gold layer were narrower in

general, due to absorption of the gold during the exposure of the SU-8. Microscope images of the waveguides seem to confirm the mentioned presumption. Since the smaller size of the waveguides increases the bend-to-bend mode overlap, the bend-to-bend transition losses were significantly reduced compared to the simulated losses. However, more experiments and simulations are needed to better understand these experimental results.

6.1 Recommendations

This work could be continued by performing similar measurements with another wafer design, containing so-called 'corner waveguides'. The characterization results of such waveguides could be analyzed together with the results presented in this thesis. This will allow distinguishing between the contributions of the total bend loss and the bend-to-bend transition loss.

The mask used for patterning the SU-8 waveguides should be adjusted such that the waveguide width in the metallic bend section equals the width in other sections. This will enable fair comparison between the metallic and non-metallic waveguides. It should be good to measure the dimensions of the fabricated waveguides (i.e. thickness and width) and adjust the simulations according to the samples that are available. Also new simulations could investigate the influence of variations in waveguide width and thickness on the bend-to-bend losses. The experiments will be easier and more accurate if the waveguides could be fabricated with a harder material than SU-8. This way the waveguides are more robust and the characterization results will be more accurate. However, fabrication of the waveguides might become more time consuming in that case.

To conclude with, the end facet quality of the waveguides can be significantly improved when they are polished with the Focused Ion Beam-technique (FIBbing). Polishing the end facets will make them all flat and identical, which is supposed to enhance in-coupling efficiency and contribute to the reliability of the experimental results. However, this is an expensive and time-consuming process as well.

7 References

[1] M. Heck, J. Bauters, M. Davenport, D. Spencer, and J. Bowers, "Ultra-low loss waveguide platform and its integration with silicon photonics," *Laser Photonics Rev.*, vol. 8, no. 5, pp. 667–686, 2014.

[2] F. Pedrotti, L. Pedrotti, and L. Pedrotti, *Introduction to Optics*, ch. 10, pp. 243 – 252. Pearson Education, Inc., 3rd ed., 2007.

[3] C. Kao, "Sand from centuries past: send future voices fast," December 2009. Nobel lecture.

[4] L. Eldada and L. Shacklette, "Advances in polymer integrated optics," *IEEE J. Sel. Topics Quantum Electron.*, vol. 6, no. 1, pp. 54–68, 2000.

[5] W. Gambling and H. Matsumura, "Propagation characteristics of curved optical fibers," *Trans. IECE Japan*, vol. 6, no. 3, pp. 196–201, 1978.

[6] A. Snyder and J. Love, *Optical Waveguide Theory*, ch. 23, pp. 475 – 483. Chapman and Hall Ltd, 1983.

[7] E. Marcatili, "Bends in optical dielectric guides," *Bell System Tech. J.*, pp. 2103–2132, 1969.

[8] S. Bozhevolnyi, V. Volkov, E. Devaux, J.-Y. Laluet, and T. Ebbesen, "Channel plasmon subwavelength waveguide components including interferometers and ring resonators," *Nature Letters*, vol. 440, pp. 508–511, 2006.

[9] M. Sefunc, M. Pollnau, and S. García-Blanco, "Low-loss sharp bends in polymer waveguides enabled by the introduction of a thin metal layer," *Opt. Express*, vol. 21, no. 24, pp. 29808–29817, 2013.

[10] H. Ma, A.-Y. Jen, and L. Dalton, "Polymer-based optical waveguides:materials, processing, and devices," *Adv. Mater.*, vol. 14, pp. 1339–1365, 2002.

[11] B. Saleh and M. Teich, *Fundamentals of Photonics*, ch. 8, p. 304. John Wiley & Sons, Inc., 2 ed., 2007.

[12] J. Saijonmaa and D. Yevick, "Beam-propagation analysis of loss in bent optical waveguides and fibers," *J. Opt. Soc. Am.*, vol. 73, pp. 1785–1791, 1983.

[13] W. Gambling, H. Matsumura, C. Ragdale, and R. Sammut, "Measurement of radiation loss in curved single-mode fibres," *Microw. Opt. Acoust.*, vol. 2, no. 4, pp. 134–140, 1978.

[14] L. Faustini and G. Martini, "Bend loss in single-mode fibers," *J. Lightw. Technol.*, vol. 15, pp. 671–679, 1997.

[15] W. Gambling, H. Hatsumura, and C. Ragdale, "Loss mechanisms in practical single-mode fibres." 4th European Conference on Optical Communication, Geneva, Sep 1978.

[16] W. Gambling, H. Matsumura, and C. Ragdale, "Curvature and microbending loss in single-mode optical fibres," *Opt. Quantum Electron.*, vol. 11, pp. 43–59, 1979.

[17] E.-G. Neumann and H.-D. Rudolph, "Radition from bends in dielectric rod transmission lines," *IEEE Trans. Microw. Theory Tech.*, vol. 23, pp. 142–149, 1975.

[18] B. Yang, L. Yang, R. Hu, Z. Sheng, and D. Dai, "Fabrication and characterization of small optical ridge waveguides based on SU-8 polymer," *J. Lightw. Technol.*, vol. 27, no. 18, pp. 4091–4096, 2009.

[19] P. V. et. al., *Algemene Practicumhandleiding*, ch. 6, pp. 50–55. University of Twente, 2011.

Acknowledgements

The work for this bachelor thesis was performed in the Optical Sciences group at the University of Twente. I very much enjoyed to be part of this group and to experience the positive atmosphere. In particular I would like to thank Mustafa Sefunc, my daily supervisor, for many helpful discussions, for motivating me and for introducing me to the art of academic writing. Also I was very happy that he gave me the opportunity to present our project with a poster at the FOM Veldhoven conference. I wish to express special gratitude to Sonia García Blanco for thinking along and giving feedback despite her maternity leave, and to Jennifer Herek for welcoming me in her group and for finding the time to take part in my graduation committee. Also I would like to thank Meindert Dijkstra: he invested a lot of time fabricating SU-8 waveguides. To Jinfeng Mu I would like to express my thanks as well for the lab training and for being available for questions at any time. Last but not least, I want to thank all other OS group members: it was really great to join you and I had a wonderful time. Thank you very much.

Willemijn van de Meent
Enschede, January 2015